Journal of Materials Chemistry A

Accepted Manuscript

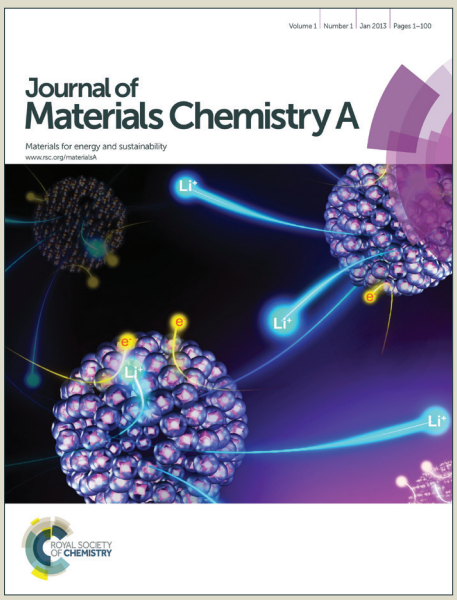

ROYAL SOCIETY OF CHEMISTRY

www.rsc.org/materialsA

Journal of Materials Chemistry RSCPublishing

ARTICLE

The role of the Ti surface roughness on the self-ordering of TiO_2 nanotubes: a detailed study of the growth mechanism

Cite this: DOI: 10.1039/xoxxoooooox

Received ooth September 2013,
Accepted ooth March 2014

DOI: 10.1039/xoxxoooooox

www.rsc.org/

A. Apolinário,[a] C. T. Sousa,[a] J. Ventura,[a] J. D. Costa,[a] D. C. Leitão,[b] J. M. Moreira,[a] J. B. Sousa,[a] L. Andrade,[c] A. M. Mendes[c] and J. P. Araújo[a]†

Highly ordered TiO_2 nanotubes (NTs) were synthesized by the electrochemical anodization of Ti foils. We extracted the effect of the Ti surface roughness (applying different pre-treatments prior to the anodization) on the length, growth rate and degree of self-organization of the obtained NT arrays. The mechanisms subjacent to the TiO_2 NTs formation and growth were correlated not only with the corresponding anodization curves but also to their appropriate derivatives (1st order) and suitable integrated and/or obtained parameters, to revel the onset and end of the different electrochemical regimes. This enables an in depth interpretation of such details (and physical-chemical insight), for different levels of surface roughness and topographic features. We found that pre-treatments that lead to an extremely small Ti surface roughness and offer enhanced NT length and also provide a significant improvement of the template organization quality (highly ordered hexagonal NTs arrays over larger areas), due to the optimized surface topography. We present a new statistical approach of evaluate highly ordered hexagonal NTs arrays areas. Large domains with ideally arranged nanotube structures represented by a hexagonal closed-packed array were obtained (6.61 μm^2), close to the smallest grain diameter of the Ti foil and three times larger than those so far reported in the literature. The use of optimized pre-treatments then allowed avoiding a second anodization step, ultimately leading to highly hexagonal self ordered samples with large organized domains at reduced time and cost.

1. Introduction

The electrochemical anodization of Ti to obtain highly-ordered nanotube (NT) arrays of anodic TiO_2 has gained much importance for a large number of applications, such as photoelectrochemical cells for H_2 production (water splitting)[1], supercapacitors[2], biosensors[3] and particularly for dye-sensitized solar cells (DSCs).[4,5] In the latter case, the 1D architecture of the TiO_2 NT structure provides a direct and efficient pathway for electrons up to the collecting electrode energy surface.[1] TiO_2 NTs can be easily obtained by electrochemical anodization of Ti in fluoride containing electrolytes. Since the first report on anodic TiO_2 NTs synthesis in dilute fluoride electrolytes by Zwilling *et al.* in 1999 (with a limited thickness of ≈ 500 nm), a great effort has been made to increase the NTs length.[6] Ethylene glycol-based electrolytes have become the main choice for the growth of long (hundreds of microns) and ordered arrays of TiO2 NTs.[7-13] More recently, NT lengths of 150 µm were obtained in 1 h of anodization with ethylene glycol electrolytes containing lactic acid.[14] However, differently from the case of Al anodization, several reports have indicated that the length of TiO_2 NTs reaches a maximum after a given anodizing time. This is attributed to the onset of additional chemical dissolution process at the NTs top and to the progressive failure of the dissolution at the NTs bottom.[9,15-19]. The TiO_2 NTs length dependence on the oxide/dissolution balances on the NTs bottom as well as the dissolution chemical dissolution on their top, is a process strongly influenced by other factors besides the electrolyte type and anodization time, namely the electrolyte concentration, pH, anodization temperature, applied potentials, that have also been studied.[7-15,20,21,22] Other studies analyzed the effect of NH_4F and H_2O concentrations (spanning 0.1-0.5 wt% and 2-15 %, respectively) in ethylene glycol-based electrolytes on the NTs length,[8,11,12,16] with the fastest growth rate obtained for 2 % of H_2O and 0.3 wt% of NH_4F.[8] Furthermore, high anodization voltages lead to longer NTs, while for low voltages the

[a] *IFIMUP and IN- Institute of Nanoscience and Nanotechnology, Departamento de Física e Astronomia, Faculdade de Ciências da Universidade do Porto, Rua do Campo Alegre, 678, 4169-007 Porto, Portugal. E-mail: jearaujo@fc.up.pt*
[b] *INESC-MN and IN, Rua Alves Redol 9, 1000-029 Lisboa, Portugal*
[c] *LEPAE- Dep. Engenharia Química-Faculdade de Engenharia, R. Dr. Roberto Frias, 4200-465 Porto, Portugal*
† Corresponding Author: jpearaujoc@fc.up.pt

chemical dissolution effects dominate the growing process and limit the NT growth.[16,17,23] However, for high-field hard anodizations (from 90 to 220 V; giving 100 µm NTs in only 4 h) the NT diameters, wall and barrier layer thicknesses greatly increase as they grow in length.[24] The diffusion path along the barrier layer oxide for the ions involved in the NTs formation is then significantly extended. This leads to a non-steady-state equilibrium between oxide formation and dissolution rate and to the deceleration of the NTs growth.[24,25]

In contrast with the factors that increase the NTs length, few studies targeted the organization and final ordering of the TiO_2 NTs in a closed-packed hexagonal array.[25,29,31,33,34] Structural order is fundamental for several applications, particularly for efficient DSCs with maximized charge transport and reduced recombination processes.[26,27] This requires an order-degree comparable to that already achieved for anodic alumina oxide (AAO) nanoporous templates (10% porosity rule).[28] In TiO_2 NTs the order is mainly influenced by the Ti foil purity, the anodization voltage[29] and the local initial surface morphology of the Ti substrate. For an irregular surface with many inter-grains, the inhomogeneous distribution of the electric field (being higher in the valleys) provides preferential sites for NT growth.[30] However, regular or periodic dimples in a valve metal can lead to an improvement of the organization degree of NT arrays, inhibiting their random nucleation. The two-step anodization process, which is crucial and mandatory to improve organization in AAO, was also used to improve the structural order of TiO_2 NT arrays.[25,29,31] On the other hand, the pre-treatment of the initial metal foil was shown to be a simple and efficient method to induce a high degree of organization in AAO templates.[32] In the TiO_2 NT arrays case, studies using pretreatments such as electropolishing (EP) or mechanical polishing (MP) indicated that a Ti smooth surface is crucial to obtain highly ordered NTs arrays since it ensures a uniform electric field distribution over the Ti surface during the anodization.[31,33-35] In particular, Lee *et al.* showed that a decrease of the surface roughness by EP leads to NTs with a more uniform length and a higher density, but almost no hexagonal NTs domains were observed.[31,33] So far high hexagonal ordering was only achieved using expensive techniques, like ion beam or nanoimprint lithography.[36,37] Furthermore, a direct correlation with the underlying formation and growth mechanisms, using a high resolution analysis of the anodization curves, was overlooked in previous reports.[8,25,31,33-36] In this work, we describe the microscopic mechanisms occurring at the TiO_2 NTs nucleation, formation and growth, which are key-issues of the degree of self-organization and growth rate. This information was extracted from a detailed interpretation of the anodization curves: current density curves $j(t)$, its derivate (dj/dt), barrier layer thickness (δ_b) and charge (Q). This procedure was systematically applied to the study of NT arrays obtained from initial Ti foils with different surface roughness (employing different pre-treatments).We were then able to achieve an integrated view on the processes underlying the formation of the NTs and their direct impact on the length and organization of the obtained arrays. We focused the factors limiting the NTs length and the critical balance between oxidation/dissolution processes, establishing a relation between these phenomena and identifiable parameters induced by the different pre-treatments employed. A new statistical methodology to characterize ordering by SEM images is presented. This work reveals a new overriding anodization parameter capable of inducing higher growth rate and improved self-organization of TiO_2 NTs arrays: the Ti surface roughness prior to the anodization, a parameter which has so far been overlooked. By tuning the Ti roughness using adequate pre-treatments, a single-step anodization readily produces highly ordered hexagonal closed-packed arrays of TiO_2 NTs with lengths above 100 µm.

2. Experimental details

Ti foils (0.127 mm thick, 99.99% purity from AlfaAesar) were ultrasonically cleaned in ethanol and deionized water for 10 minutes. Prior to the anodization, three different pre-treatments were performed on 1 cm^2 pieces of the as-rolled (AR) Ti foil:
(i) Chemical etching (CE) in a 4 % (wt %) HF aqueous solution during 15 min at room temperature;[24]
(ii) Mechanical polishing (MP) on a plane disc at 150 rpm in three steps of 10 min each. In the first two steps we used an ultrapol-cloth with 6 and 3 µm diamond particles suspension; in the third step a silica colloidal suspension (0.05 µm) with H_2O_2 (30 % concentration in volume) on a microcloth was used;
(iii) Electropolishing (EP) in a H_2SO_4/HF (8:3) solution, with an applied potential of 10 V between the Ti foil and an inert Pt mesh (distance 2.5 cm) for 4 min; the solution was mechanically stirred (300 rpm) and kept at room temperature.[40]
After each pre-treatment the corresponding Ti foil samples, as well as an AR Ti sample without treatment, were analyzed using a *Nanoscope Multimode Atomic Force Microscope* from *Veeco Instruments* to extract the surface roughness (*Rq*). Subsequently, the samples were electrochemically anodized in an in-house made anodization cell (two-electrodes), where the Ti acted as the anode and an inert Pt mesh was used as cathode. The time evolution of the current density [$j(t)$] was monitored during the anodization using a *Keithley 2004 Sourcemeter* remotely controlled by a *LabView* application (using 100 ms aquisition step in the first 5 min). The electrochemical anodization was carried out for each sample at a constant potential of 60 V for 17 h, in a freshly prepared ethylene glycol solution containing NH_4F (0.3 wt %) and H_2O (2 wt %) at room temperature with mechanical stirring.[8] The NTs morphology was evaluated by a *FEI Quanta 400FEG Field Emission Scanning Electron Microscopy* (SEM) using the cross-sections (for the NTs length calculation) and surface top and bottom views. The bottom views were prepared by natural peeling-off, becoming a free-standing non-curling membrane (detachment occurs without any assistance or other methods as described elsewhere).[27,41] From the SEM images, a statistical analysis was performed enabling a quantitative evaluation of the organization pattern and NT structure dimensions.

3. Results and Discussion

3.1 Ti surface topography analyses

The surface topography of the Ti samples with different pre-treatments (and one as-rolled) was investigated by Atomic Force Microscopy (AFM). Figure 1 shows representative 1 μm^2 images of such Ti surfaces. The average surface roughness was extracted from the topography, defined as the root-mean-square value of the images pixel height. The AR sample presents a significant surface roughness of 8.3 nm [Fig. 1(a)]. After the CE pre-treatment, the Ti foil showed a highly damaged surface, characteristic of a chemical attack, giving a higher etching rate on surface defects, namely grain boundaries.[34] This led to the highest *Rq* value of all the studied samples [37 nm; Fig. 1 (b)]. In contrast, a significantly smoother surface was obtained in the MP and EP samples with *Rq* of 1.0 nm and 2.4 nm, respectively [Fig. 1(c) and (d)]. With the MP pre-treatment, the Ti

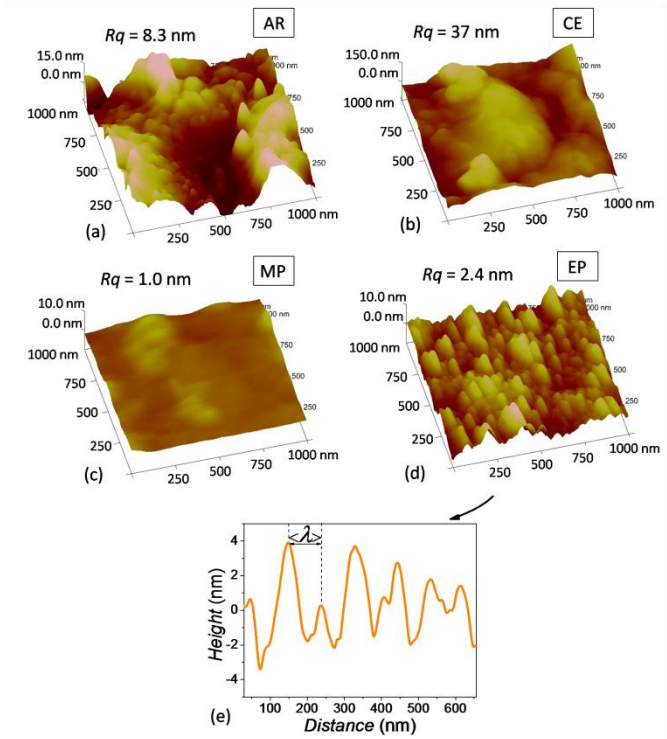

Fig.1 Ti surface topography prior to the anodization obtained using AFM and corresponding *Rq*: (a) as-rolled, (b) chemical etching, (c) mechanical polishing and (d) electropolishing; (e) profile height for the EP sample.

foil surface became smooth and fairly plane. On the other hand, the Ti surface after EP revealed a dimple-pattern structure. This shallow ripple-like structure is an EP characteristic on metals[40] and can be used as a pre-pattern prior to the anodization to obtain highly ordered oxide nanostructures, as shown in the case of Al.[32,40,42-45] The electrochemical polishing of Ti is usually achieved in sulphuric acid-based electrolytes, which results in smooth surfaces.[46] However, in this work the EP conditions used (electrolyte type and voltage) resulted in organized dimple patterns[40], with an inter-ripple spacial period $<\lambda> = 97$ nm [Fig. 1(e)].

3.2 Growth mechanisms of anodization current density curves

The mechanisms that lead to the formation and growth of the NTs can be monitored during the anodization process by the current density curves and the corresponding time derivative, as shown for the EP sample in Figs. 2(a) and (b). The evolution of the TiO_2 barrier layer thickness (δ_b) at the bottom of the NTs was also estimated from the j(t) curve [Fig. 2(c)]. According to the high-field conduction theory, the current density (j) is related to the voltage (V) drop across the barrier layer as follows:

$$j = \alpha e^{\beta \frac{V}{\delta_b}} \quad , \qquad (1)$$

where α and β are electrolyte and material dependent constants (2.4×10^{-37} A. nm^{-2} and 56 nm.V^{-1}, at room temperature respectively) and the (V/δ_b) ratio is the effective electric-field across δ_b.[16,25,47] From Eq (1) we obtain,

$$\delta_b = \frac{\beta V}{\ln\left(\frac{j}{\alpha}\right)} \quad , \qquad (2)$$

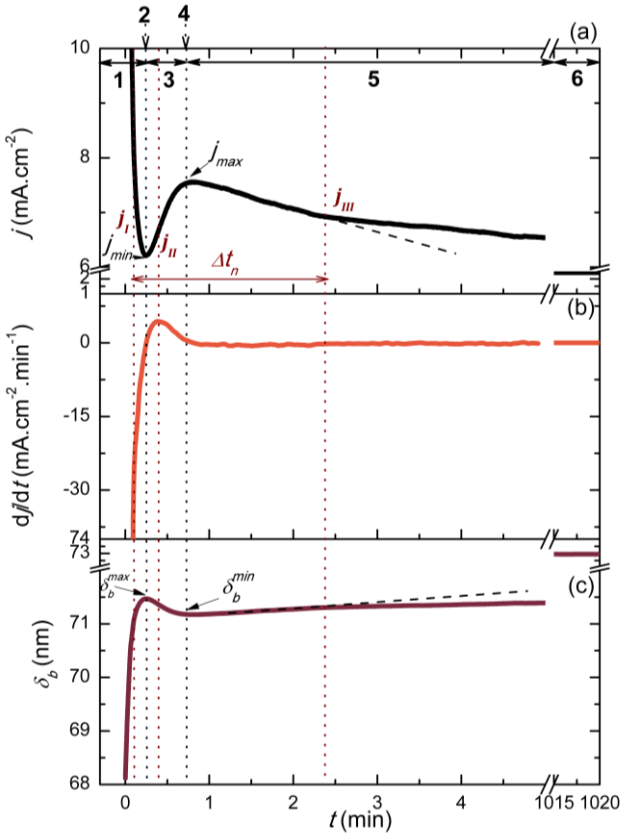

Fig.2 (a) Transient period of the anodization curves for the EP sample; (b) the corresponding derivate and (c) δ_b associated with different stages of the TiO_2 NTs growth mechanisms.

during the anodization. Note that even if the effective area changes during the anodization, its impact on the extracted value δ_b is small, justifying the use of Eq.(1).

Since the electrical resistance (R) across the Pt electrode – electrolyte – Ti electrode is initially small, the current density starts with a large value, $j(t \approx 0) \approx 65$ mA·cm^{-2} [Fig. 2(a)]. Then, a continuous TiO_2 barrier layer is rapidly formed, substantially increasing R (rapid j decrease; stage 1) until a minimum (j_{min}) is reached (stage 2). This minimum corresponds to the maximum of δ_b. The subsequent increase of j (stage 3) indicates a δ_b decrease, which persists until j reaches a maximum (j_{max}) and δ_b reaches a local minimum (stage 4). From this point onwards new electrochemical processes come into play, as evidenced by the slow j decrease, indicating a slow-rate increase of δ_b (stage 5).

Commonly, j_{min} is associated with the onset of NT nucleation,[38] likely on the surface valley-type irregularities, where the higher electric field enhances oxide dissolution and hole formation. To deeply study the effects of topography on NT nucleation and growth, high resolution measurements of the time derivative (dj/dt *vs* t) were used to investigate the subtle features present in $j(t)$ [Fig. 2(b)]. One sees that dj/dt exhibits no singularity or change of behavior at $j = j_{min}$ and thus j_{min} cannot represent the beginning of the nucleation stage. In fact, considerably before reaching j_{min} [j_I in Fig.2(a)], dj/dt significantly slows down likely reflecting early random nucleation and pore formation by chemical dissolution (F^- ions) in favorable

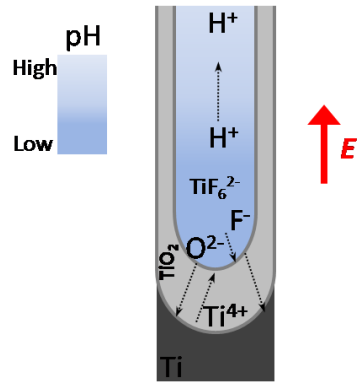

$H_2O \rightarrow 2H^+ + O^{2-}$

$Ti + 2O^{2-} \rightarrow TiO_2 + 4e^-$ (oxidation)

$TiO_2 + 6F^- + 4H^+ \rightarrow TiF_6^{2-} + H_2O$ (dissolution)

Fig. 3 Schematic diagram illustrating the ions diffusion profiles inside the NTs during the anodization. The dissolution of TiO_2 occurs at both the top and the bottom of the NTs, while the oxidation occurs only at the bottom.

spots of the TiO_2 surface.[48] Although δ_b is still increasing [Fig. 2(c)], indicating Ti oxidation dominance, the progressive emergence of the pores (the local dissolution of δ_b gradually increases) reduces the effective barrier resistance-rate increase. There is then a competition between electrochemical Ti oxidation (increasing R) at the Ti/oxide interface and TiO_2 dissolution (lowering R) at the oxide/electrolyte interface. Accordingly j_{min} marks the balance between the two processes,, thus the limiting oxide thickness (δ_b^{max}). In other words, oxidation is weakened by the increase of δ_b, which progressively restrains O^{2-} electromigration through the thick TiO_2barrier, whereas the F^- dissolution processes continue smoothly at the TiO_2/electrolyte interface (Fig. 3). Consequently, δ_b decreases after j_{min} (smaller rate of Ti oxidation), while the tubes formation accelerates, as evidenced by the increase of dj/dt up to the $j(t)$ inflexion point at j_{II} (maximum dj/dt). It is likely that a sufficient number of NTs already exists at j_{II}, but the tubes-formation process goes on until it effectively eliminates the available oxide regions for nucleation. Ultimately, saturation occurs at j_{max}, where dj/dt =0 (and δ_b is minimum). From this point onwards, the incipient NTs adjust and compete among themselves to improve the degree of order in a self-organized process. In this stage, δ_b slightly increases, particularly between j_{max} and j_{III}, which marks the onset of a new regime. Notice that the nucleation time can now be defined as $\Delta t_n = t_{nIII} - t_{nI}$, where t_{nIII} marks the kink at j_{III} and t_{nI} marks the beginning of nucleation at j_I. As the anodization proceeds, the formed NTs grow at a constant rate and δ_b would remain constant if Ti oxidation balanced oxide dissolution.[7,8,12,15] However, at this stage ($j < j_{III}$), the oxidation/dissolution processes are not quite in equilibrium, being the TiO_2 dissolution lower than its formation. This results in a smooth increase of δ_b after the j_{III} kink and the consequent slow decay of $j(t)$ (stage 5). This is related with the lack of F^- ions at the NT bottoms, since they are difficult to replace by fresh ones due to the high viscosity of the electrolyte. As the NTs grow, large diffusion distances (lengths) must be travelled and thus longer times are required to renew the F^- concentration at the pore bottom. Consequently, the oxidation at this stage becomes higher than the dissolution, leading to an increase of δ_b that further inhibits the transport of F^-,Ti^{4+} and O^{2-} ions across the barrier[12] (Fig. 3) and further limits NT growth (stage 6).

Growth mechanisms for different levels of roughness. The $j(t)$

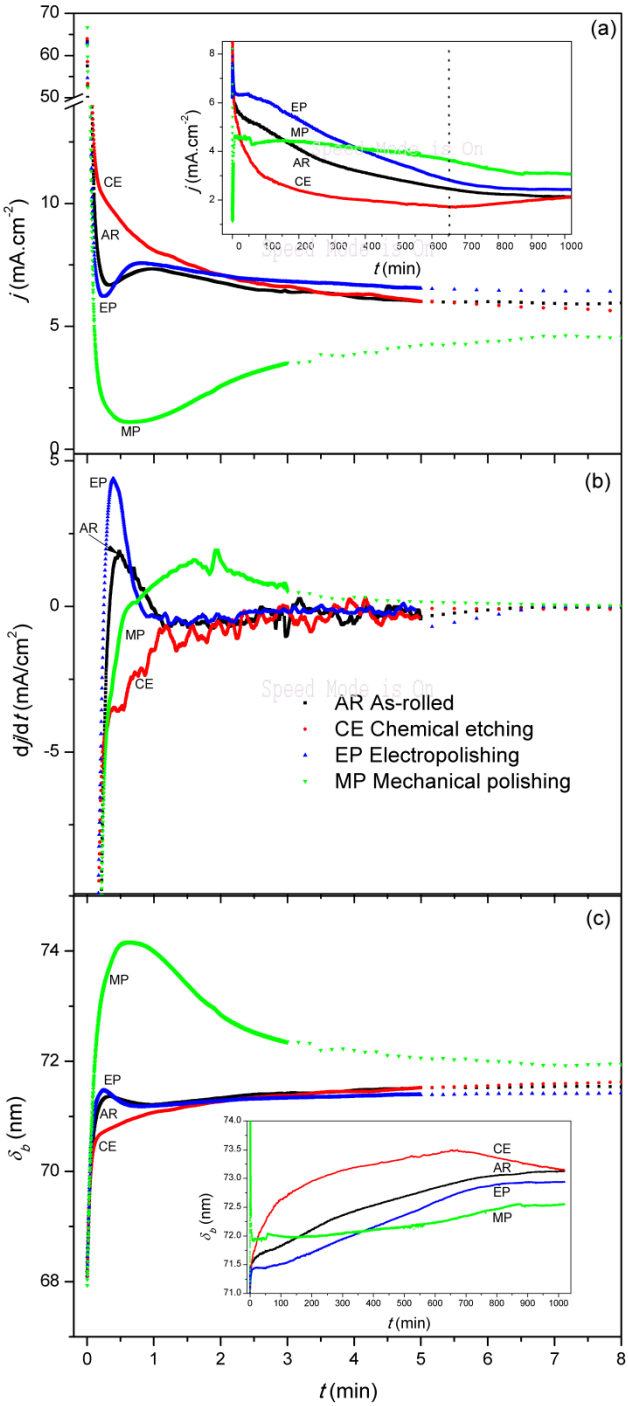

Fig. 4 (a) Current density anodization curve transient for 8 min of anodization (inset: 17 h of anodization); (b) corresponding derivatives; (c) TiO_2 barrier layer thickness (δ_b) for 8 min of anodization (inset: 17 h of anodization) for the AR, CE, MP and EP samples.

curves of the samples subjected to the different pre-treatments used in this work are shown in Fig. 4(a). The $j(t)$ transient of the MP sample substantially differs from all others in two critical aspects: i) an extended period of time over which low-rate pore nucleation smoothly takes place and ii) the fairly small $j(t)$ values over such region, indicating the growth of a thicker TiO_2 barrier layer [Fig. 4(c)]. This is at first sight unexpected when compared to the EP sample, which presents similar Rq values

(2.4 nm *versus* 1.0 nm of the MP sample). However, the MP sample has an almost flat and smooth surface, whereas the EP surface reveals unique periodical rippled structures [Figs. 1(d) and (e)]. These ripple structures act as nucleation points (valleys) so that nucleation occurs simultaneously on many sites, making the overall nucleation time fairly short. In opposition, the lack of topographic irregularities in the MP sample leads to longer nucleation times (longer Δt_n) and fairly low j_{min} value (~ 1.5 mA·cm^{-2}), i.e. a thicker δ_b. The rapid dissolution rate in the EP sample is clearly observed in the dj/dt and δ_b curves [Fig. 4(b) and (c)]: after j_{min} the pore dissolution accelerates as δ_b decreases, with dj/dt rapidly reaching its maximum value at the inflexion point (j_{II}), appearing much earlier than for the MP sample. Additionally, the MP sample exhibits a much higher and broader δ_b^{max} peak [Fig. 4(c)], confirming the much slower dissolution rate during the porous formation. The consequence is the absence of the typical shoulder-like behavior in $j(t)$ ascribed to the competition between growing NTs and consequent organization quality,[32,39] being more readily organized during the slow oxide-dissolution process. On the other hand, in the EP sample the vigorous faint dissolution rapidly leads to a pronounced j_{max} and a shoulder-like trend. Furthermore, in the inset of Fig. 4(c) we notice that at the end of the anodization, samples with lower *Rq* (MP and EP) exhibit a final δ_b-value lower than samples with higher Rq (CE and AR)." Fig. 5 shows a STEM image of the MP sample, with δ_b = 73 nm, in excellent accordance with the value obtained using the curve $\delta_b(t)$ [Fig.4(c)] after 17 h of anodization.The $j(t)$ curve of the AR sample presents a similar shape as that of the EP sample, *i.e.* a smaller Δt_n despite its larger *Rq*. This shows that both samples have enough easy-nucleation spots related with the topographic valleys. Nevertheless, the ripple EP valley structure favors earlier and faster organized nucleation (smaller Δt_n) than the broader random valleys of the AR sample. The previous analysis of the anodization curves of the MP, EP and AR samples clearly reveal the importance of the surface topography details (smooth, ripple-like and random broad valleys) in promoting effective nucleation spots and thus the earlier emergence of NT nucleation and lower Δt_n: Δt_n(EP) < Δt_n(AR) < Δt_n(MP). Figure 6 shows j_{min} and j_{max} - j_{min} as a function of *Rq* for the AR, EP and MP samples. With the decrease of *Rq*, j_{min} also decreases and higher j_{max} - j_{min} values are reached. Therefore, Ti surfaces with lower *Rq* lead to higher TiO_2 oxide barriers (δ_b^{max}) and quality, since less defects are present in the primordial Ti surface, and the dominant oxidation process [at stage (1)] delays dissolution. Moreover, lower *Rq* leads to thinner δ_b^{min} and δ_b during the anodization, which allows higher $j(t)$ (due to a more uniform and optimized electric field and current) and consequently an increase of the NTs growth rate.

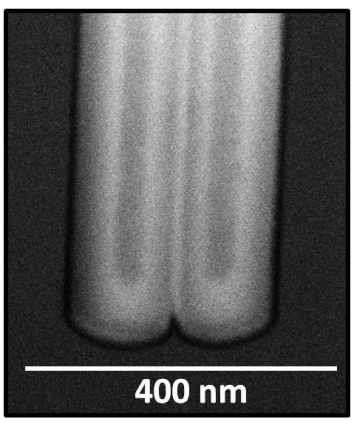

Fig. 5 Measurements of δ_b after 17h of anodization for sample MP in STEM Transmission - mode.

The particular case of high roughness. The sample pre-treated with CE shows a different $j(t)$ behavior from those previously discussed (or shown in the literature) due to severe chemical etching effects (rise of *Rq* from 8.3 nm to 37 nm; see Fig. 1). In particular, it is difficult to directly extract key-values such as Δt_n from the $j(t)$ curves. One simply observes a monotonic decrease of j along the whole anodization period, indicative of stronger oxidation than dissolution processes. This explains the absence of the typical transient period with nucleation and dissolution stages, as well as j_{max} and j_{min}. The AFM topographic imaging was performed after 17h of anodization and after removal of the TiO_2 NTs template (Fig. 7). The Ti surface revealed the characteristic pre-pattern left by the NTs, but different areas of organization and depth can be observed [zones 1 and 2 in Fig. 6(a)]. The regions with higher depth (zone 2), reached a higher anodization growth rate since these areas correspond to the primordial etched Ti surface with valleys (topographic minima). In contrast, the regions with hills had a lower anodization growth rate and showing a lower depth (zone 1). Therefore, the measured macroscopic $j(t)$ curve has contributions from the many different anodization zones.

3.3 Growth rate of anodization charge curves

Figure 8 shows the charge curves $Q(t)$ obtained from the $j(t)$ data. The $Q(t)$ curves of all samples present non-linear shapes characteristic of non-steady state processes. The decrease of the slope during the Ti anodization occurs due to the lack of an oxidation-dissolution balance (Ti oxidation is higher than TiO_2 dissolution) that leads to an increase of δ_b as the anodization proceeds [Fig. 4 (c)].
The $Q(t)$ slope of the EP and MP samples is higher than that of AR and CE samples for the entire anodization period (Fig. 8). This behavior is related with the steady-state balance between the oxidation and dissolution processes in the EP and MP samples. Even though the MP and EP samples have almost the same final charge transfer of 3900 C after 17 h, the slope's trend is significantly different: whereas $Q(t)$ behavior in MP sample is rather linear, providing an almost constant rate growth, the EP presents two distinct growth regimes. After 500 min of anodization time, the growth rate of the EP sample slows down due to the thicker δ_b [Fig. 4(c)] ultimately being surpassed by the MP sample.
The charge transferred during the anodization process was found to be related with the surface *Rq*. Lower *Rq* samples present higher j(t)

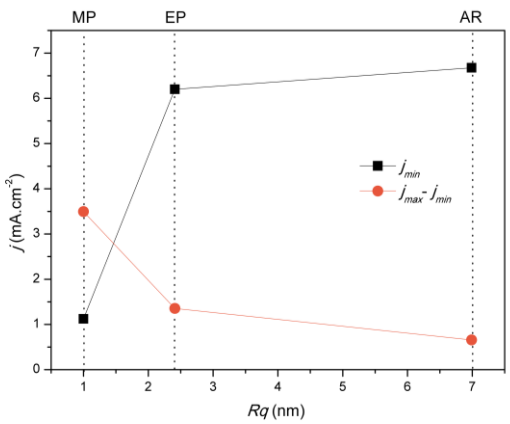

Fig. 6 j_{min} *and* j_{max} - j_{min} values as a function of the surface roughness for: AR, EP and MP samples.

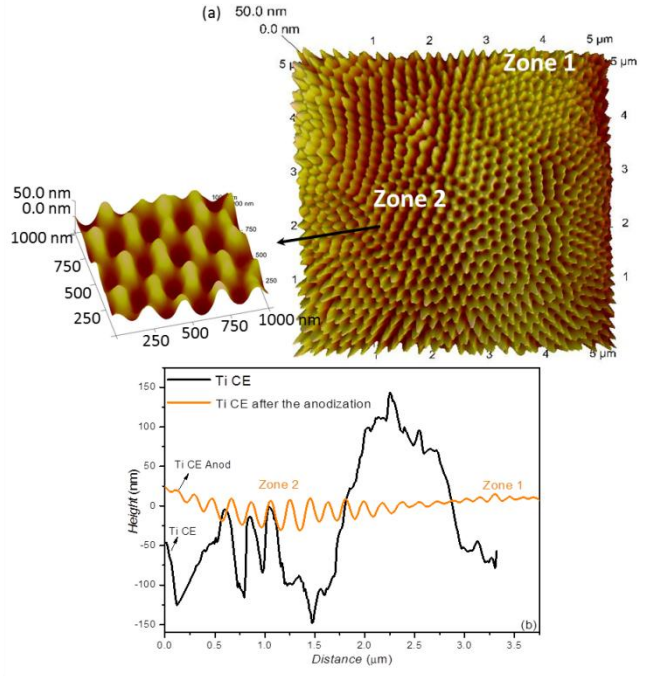

Fig. 7 (a) AFM image of the Ti surface of CE sample after 17 h of anodization and removal of the TiO_2 NTs template; after the anodization the Ti surface reveals the NTs arrays hexagonal pattern. There are two different zones with different growth rates: zone 1 with a slower anodization growth rate and zone 2 with higher anodization growth rate; (b) corresponding section of the height profile.

and Q(t) values, since is reached a more homogeneous electric field over the whole sample, originating an oxidation/dissolution process more equally balanced and delaying the additional chemical effects that limit NTs growth. As a higher final $Q(t)$ indicate higher NTs template thickness (L), one expects L(MP) > L(EP) > L(AR) > L(CE).

3.4 Nanotubes growth

Figure 9 shows SEM cross-section and top view images of the NT templates for all samples after 17 h of anodization. The resulting template thicknesses are shown in Table 1. The AR sample has a mean NT template thickness (<L>) of approximately 89 μm, while the CE sample has <L> = 83 μm. On the other hand, the EP and MP samples show a rapid NT growth and enhanced mean lengths of 125 μm and 128 μm**,** respectively, *i.e.* a length increase of over 40% when compared with the AR and CE samples.

Comparing <L> with the Rq results, one can infer that the surface topography is directly correlated with the NTs growth and template thickness (Fig. 10). In fact, the pre-anodizing surface conditions are crucial to reach higher growth rates and thicker NTs, *i.e.* by decreasing Rq, longer NTs are obtained. It is important to notice that the large Rq value of the CE sample is responsible for the decrease of the NTs growth rate and length up to 660 min anodization time. However, due to the acidity increase of the electrolyte at the NTs top (top dissolution), the F^- ions can then more easily reach the NTs bottom, being readily available to again increase the NTs growth rate. This is clearly seen in the j(t) curve presented in the inset of Fig. 4(a), where a j increase is observed at t = 660 min, indicating that L restarts to increase. The enhancement of the growth rate concerning samples EP and MP should result from the decrease of Rq and the presence of small nucleation sites (see Fig. 11).

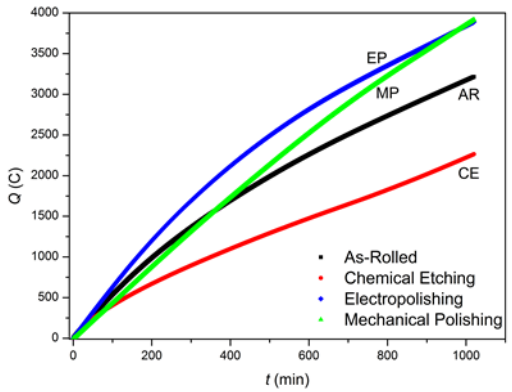

Fig. 8 Charge [$Q(t)$] curves obtained by integrating the $j(t)$ anodization curves of the studied AR,CE, MP and EP samples the EP sample slows down due to the thicker δ_b [Fig. 4(c) inset] ultimately being surpassed by the MP sample.

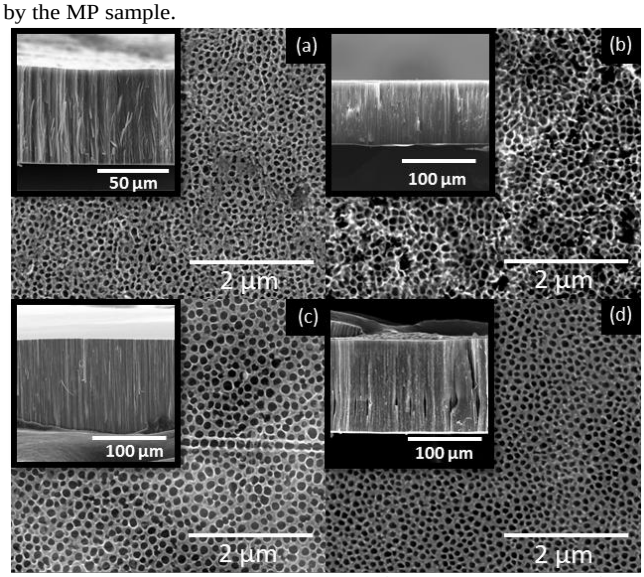

Fig. 9 Top view and cross-section (insets) of the TiO_2 NT templates from the different samples after the 17 h of anodization: (a) AR Ti foil, (b) CE, (c) MP and (e) EP.

Table 1. TiO_2 NTs template thickness results: mean <L> and the maximum L_{max} length

	AR	CE	MP	EP
<L> (μm)	88.93	82.50	128.33	124.77
L_{max} (μm)	91.50	85.00	130.50	126.50

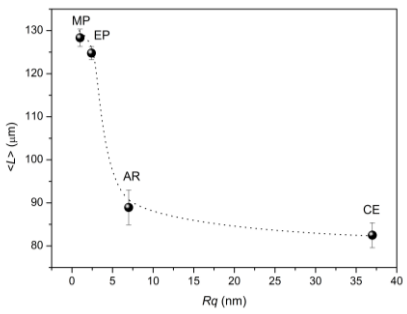

Fig. 10 TiO_2 NT template thickness average (<L>) as a function of the Ti surface Rq.

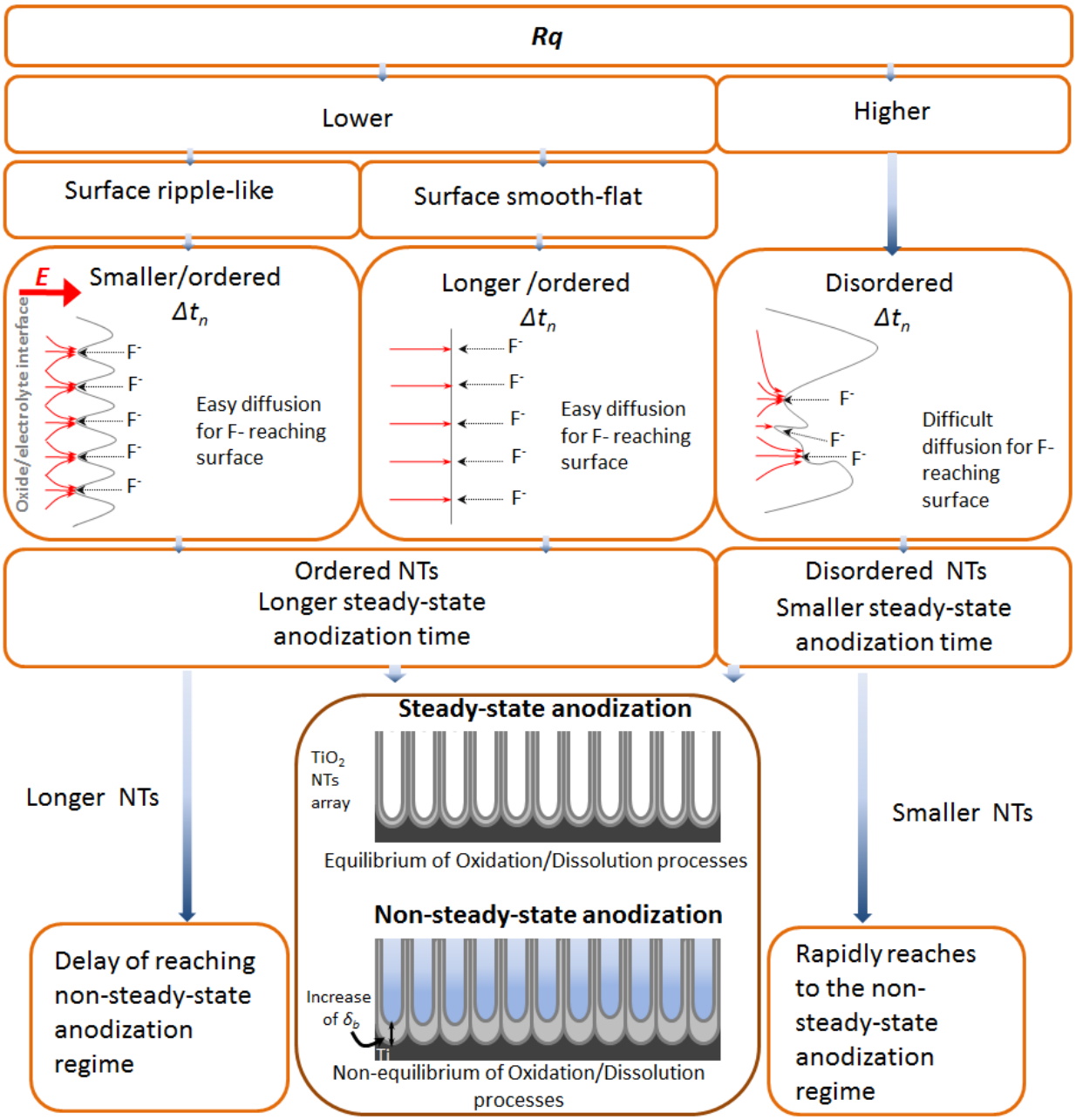

Fig.11 Schematic diagram illustrating the influence of the Ti surface *Rq* (prior to the anodization) and topography on the growth mechanisms at the nucleation stage, NT ordering and length. To have longer and more ordered NTs a steady-state anodization, that delays the δ_b increase, is crucial.

A smoother surface favors to the mobility of ions in the dominant anodization processes, promoting greater accessibility of F^- ions that reach the Ti surface and thus favoring the dissolution processes. On the other hand, the additional chemical effects (namely pH increase throughout the anodization) are retarded since the anodization growth limit (*i.e.* when oxidation surpasses the dissolution, causing a thick δ_b) is delayed. Also, for samples with low *Rq*, the δ_b increase during the anodization is slower [inset of Fig. 4(c)], which promotes ions electromigration (F^- and O^{2-}) through the δ_b, fundamental for the dissolution/oxidation balance processes. This is clearly visible in the MP and EP samples (*Rq* of 1 and 2.4 nm, respectively) that reach a template thickness enhancement of over 40 %, keeping an almost intact oxide nucleation layer after 17 h of anodization.

3.5 Nanotubes array organization

To reveal the degree of organization of the produced NT arrays, we performed a statistical evaluation of SEM images (25 000 x) of the NT templates bottoms in a random area of each sample. Since the analyses of the top surface would shows the initial random nucleation pores, the bottom analyses arises as a more adequate technique to evaluate the degree of organization.[29,33]
Based on this analysis the following parameters were quantified: (i) the NTs hexagonal domain area (delimited area where the NTs have a hexagonal arrangement); (ii) the organized area (% organized

area/total evaluated area); and (iii) the NTs density (number of NTs per unit area) and NTs diameter distribution.

NTs hexagonal domain area. The degree of order of the NT domains as a function of their hexagonal arrangement and individual shape was analyzed.[29] The NTs organization increases as the NTs tend to pack themselves in a closed-packed hexagonal arrangement, leading to tubes with a hexagonal section. The deviations from this shape due to Ti defects and grain boundaries result in pentagons, heptagons or circular shapes.[29] To quantify the order-degree of the domains, they were first classified in two types of classes: Class 1 has a lower order-degree domain with an ideal Hexagonal Closed-Packed Array (HCPA) structure, exhibiting NTs with diverse polygon shapes other than hexagonal; Class 2 domains having a higher order-degree domain with the same HCPA structure, but each NT exhibiting a hexagonal shape (Fig. 12). To calculate the domain areas, the HCPA areas of each SEM image were delimited and labeled using *ImageJ*.[49] Figure 13 shows SEM images of the bottoms of the NT layers of each sample (AR, CE, MP and EP). For each SEM image, besides the delimitation of these HCPA domains, the maximum sized ones were differently colored as Class 1 (orange) and Class 2 (green). Figure 14 displays the statistical results of the analyzed SEM images. The CE sample displays large areas with completely disorganized NT arrays (darker areas) of small diameter [Figs 13(b) and (f)]. Therefore, for the CE sample the statistical calculations were only possible on the small areas with NTs of large diameters, where some degree of organization occurs [inset of Fig. 13(b)]. These domains correspond to the valleys present in the Ti foils after the CE pre-treatment (see AFM images in Fig. 7) where the anodization rate is higher. In this sample, the obtained ordered array size presents an average value of 0.92 μm^2. However, the organized area represents only 75 % of the total area from the considered SEM image. The AR, MP and EP samples have the same organized area fraction (~ 96 %), with the MP and EP samples clearly having larger average domain sizes (0.80 and 0.92 μm^2, respectively) than AR sample (0.50 μm^2).Note that, while the AR sample presents a Class 1 maximum domain size of 1.8 μm^2, the EP and MP samples show much larger Class 2 maximum domain sizes (6.61 and 4.32 μm^2, respectively). Therefore, a clear improvement of the NTs quality an organization was obtained with the simple application of pre-treatments such as EP and MP in the Ti foil before anodization. The most relevant improvement found was the increase of the Class 2 domain size from the EP sample. It is also important to mention that the area for the Class 2 domains in the EP sample (or even in the MP sample) largely exceeds the maximum value reported in the literature of 1.83 μm^2 [25] (or in the case of nanoporous templates structures the reported domain area is about 0.25~1μm^2) [31]. In fact, the use of these pre-treatments pushed NT domain sizes close to the smallest grain diameter of commercial Ti sheets (5 to 50 µm on average).[50]

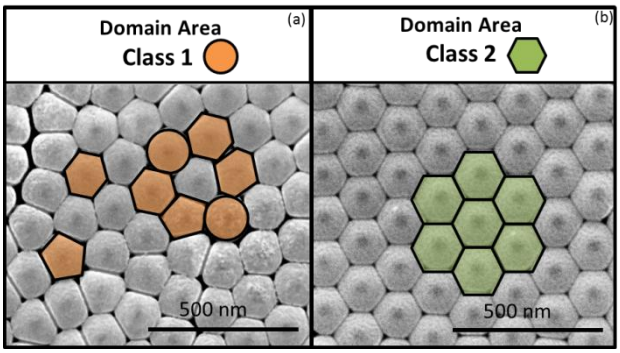

Fig. 12 Bottom TiO_2 NTs for the two different classes. (a) Class 1: lower order (hexagonal arrangement; NTs without a hexagonal shape), (b) Class 2: higher order (hexagonal arrangement; NTs with a hexagonal shape.

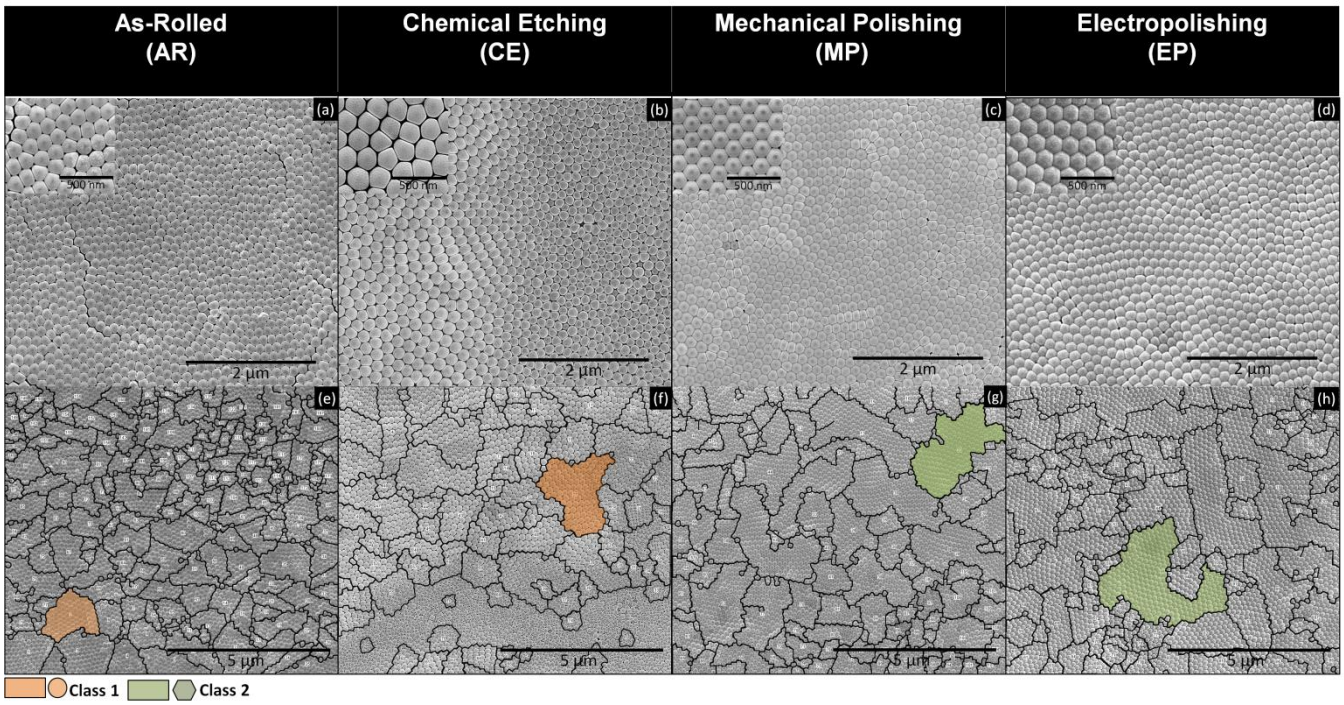

Fig. 13 SEM images of the TiO2 NT bottoms from the different samples: (a) AR, (b) CE, (c) MP and (e) EP. For each sample, a SEM image was analyzed [(e), (f), (g) and (h)]: the domains areas (µm2) were delimited, labeled (not readable small white labels within each domain) and the maximum domain area in the image colored with the corresponding class types (Class 1 and Class 2)

NTs density: number of NTs per unit area and NT diameters. Figure 15 shows the results of the NTs density and diameter (*D*) of the studied samples. The average diameter was estimated from the histogram of the size distribution, which was then fitted to a log-normal distribution (inset of Fig. 15). The decrease of *Rq* in the MP and EP samples leads to a decrease in the NTs density since *D* increases. The NTs density is therefore also determined by the Ti *Rq* prior to the anodization. According to this relation one would expect that the EP sample, which has a slightly higher *Rq* than the MP sample, to have a higher NT density (and a slightly smaller *D*). The observed smaller density of the EP sample is related with the fact this sample has NT arrays with less space between the hexagon corners than the MP sample. Remember that the EP sample surface showed a pattern with small ripple-like structures, which act as nucleation points on the valleys, forcing the nucleation to occur simultaneously in an organized manner. Since this periodical structure has a spacial period of $\langle\lambda\rangle$ = 97 nm (D ~157 nm), each valley behaves as a single nucleation site. The NTs then turn to be more packed and with slightly higher diameters due to an increase of the current flowing through these sites. Thus, almost no competition exists between the NTs, resulting in optimized structures. As for the CE sample, the darker disorganized regions correspond to NTs with small diameters (*D* = 130 nm and σ = 29.4 nm) and a NT density of 57 NTs/μm^2. On the other hand, the highly organized areas (zone 2) have NTs with much larger *D* (196 nm and σ = 0.286 nm) and density of 32 NTs/μm^2. This increase of the diameter is associated with the surface topography that increases the electric field in the valleys-sites.

In the case of the CE sample, the previously mentioned trend of increasing *D* (and consequently the NTs density) with decreasing *Rq* (Fig. 14), is not completely valid. Although non-organized areas indeed show the expected trend, in the organized areas the *Rq* increase leads to an increase in *D*. Remember the special behavior of this sample ("The particular case of chemical etching" on subsection), where two different areas cause different anodization conditions and consequently NTs organization, diameters and density. Indeed, Raja *et al.* suggested that pore ordering originates from the effect of local surface perturbations that causes the increase of the strain energy, *i.e.* electrostriction, electrostatic and recrystallization stresses at the valleys.[51] Since the surface energy acts as a stabilizing force on a plane surface, when perturbed by a sinusoidal morphology the energy density varies across the hills and valleys, showing higher stress concentration and strain energy on the latter and leading to F^- migration and adsorption where the NTs structure first occurs. Thus, due to the periodic perturbations of such ripples, the electric field is higher on the valleys, which results in NT growth in these sites. Therefore, one of the main achievements of this study is the experimental proof that the NTs diameter is not only associated with the anodization potential but also with the Ti surface conditions.

Electropolishing as one step anodization route. MP and EP pre-treatments led to the best results, both regarding the total NTs length and their level of organization. Nevertheless, to achieve MP samples with a high level of smoothness (*Rq* ~ 1 nm) is a long and expensive process with low reproducibility. In this context, the EP process becomes more attractive and easy to perform. Despite not leading to the smallest *Rq* values, the EP pre-treatment actually facilitates NT growth and organization due to the intrinsic formation of the periodic ripples pre-patterned in the Ti surface. This process is similar to the two-step anodization where the dimple pattern left by the first anodization is crucial to achieve the ideal hexagonal ordering in the second step.[38] These dimples on the Ti surface act as initiation sites for tube growth and thus may well be a pre-condition to obtain extended order.

Macak *et al.* showed that performing two step anodization on Ti foils significantly improves the hexagonal ordering, decreasing the number of packing errors (pentagons, heptagons etc.), although further increases the number of anodization steps.[29] In the present work, we explained that MP and EP pre-treatments successfully led to the best results: NTs length and their level of organization, avoiding the second anodization. However, to achieve MP samples with a high level of smoothness (*Rq* ~ 1 nm) is a long, hard-work and expensive process with low reproducibility. The use of an EP pre-treatment leads to highly hexagonal self-ordered samples with large domains of organization at a reduced time and cost. In this context, the EP process becomes more attractive and easy to perform.

Furthermore, the degree of ordered can be evaluated calculating the porosity (*P*) of the NTs arrays. For an ideal hexagonal arrangement

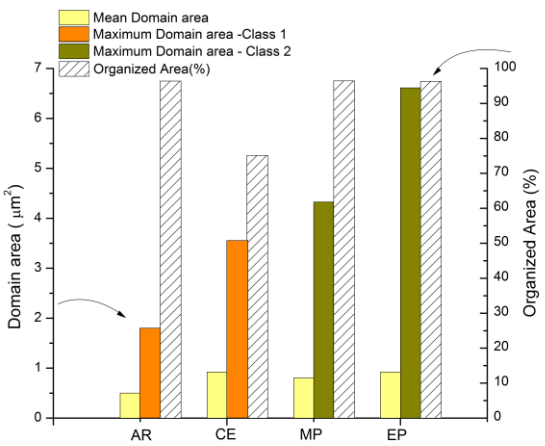

Fig. 14 Statistical results of the analyzed NT bottom SEM images for the different samples, indicating the results obtained for the mean and maximum domain areas (Class 1 and Class 2) and the organized area (%).

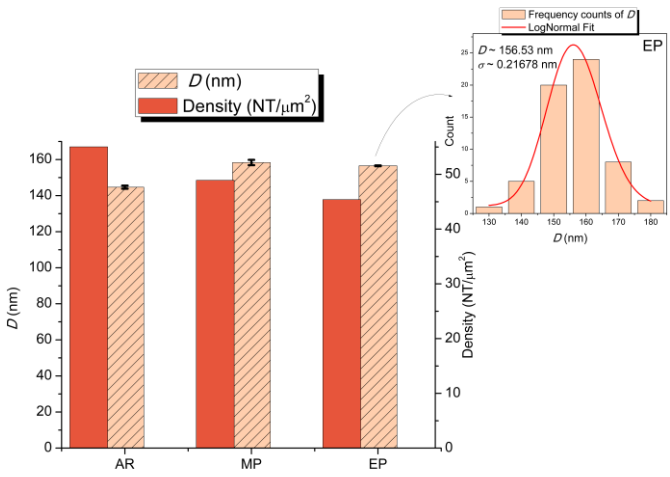

Fig. 15 Density [number of NTs per area (NTs/μm^2)], NTs diameter (*D*) and standard deviation (σ) for the AR, MP and EP samples. *D* and σ were calculated by performing an histogram of the NTs diameter distribution and a log-normal fit; the upper inset shows the NTs *D* histogram and log-normal fit of the EP sample.

of pores, P can be estimated using:

$$P = \frac{2\pi}{\sqrt{3}}\left(\frac{(D_p/2)}{D_{int}}\right)^2, \qquad (3)$$

where the pore diameter is $D_p = 2r$ and D_{int} is the interpore distance. Using *ImageJ* we calculated a mean wall thickness of $w \sim 51.78$ nm (SEM image of MP sample of Fig. 5) and with the external diameter previously extracted from the histogram analyses (D =158.3 nm), we obtain the internal diameter D_p = 54.78 nm. Due to the hexagonal geometry, we considered the interpore distance (D_{int}) equal to the external diameter ($D = D_{int}$). Using Eq (3), D_p = 54.8 nm and D_{int} = 158.3 nm, we obtain a porosity of $P \sim 10.8\%$. The NT templates thus present a porosity close to the 10% benchmark reported for the self-organized-regime in AAO templates.[28]

The closed-packed hexagonal structure with a degree of order comparable to that of AAO templates was not reported so far for TiO_2 templates. Comparing the results achieved in this work with the already reported domains of 1.83 μm^2 with 20 % of porosity,[25] the proposed approach contributes for the improvement of both ordered (HCP) domain areas and porosity of hexagonal arrays of TiO_2 nanotubes.

4. Conclusions

By bonding the formation and growth mechanisms of the TiO_2 NTs with the analyses of the anodization curves, this work reveals a new overriding anodization parameter, the Ti surface roughness, capable of inducing higher growth rate (extended NTs length) and improved self-organization.

The analyses of the anodization curves, $j(t)$, dj/dt and $Q(t)$, clearly revealed the importance of the surface topography details: ripple-like (EP) and random broad (AR) valleys promote effective nucleation spots and thus the earlier emergence of NT nucleation and lower Δt_n than a smoother topography (MP). Furthermore, the samples with lower *Rq* (and the presence of small nucleation sites) show an uniform enhancement of the growth rate as well as highly organized array. With a lower surface *Rq*, we obtain a more homogeneous electric field over the sample surface, causing a thinner δ_b which promotes ionic electromigration (F^- and O^{2-}) through δ_b. This is fundamental for the dissolution/oxidation balance in a steady state anodization. Indeed, samples with smoother surface *Rq* (MP and EP) presented higher $j(t)$ and $Q(t)$, a thinner δ_b and a smaller $\delta_b(t)$ increase during the anodization. Furthermore, a smoother surface promotes a higher mobility of F^- ions in the dominant anodization processes, promoting greater accessibility of F^- ions to reach the Ti surface (and thus favoring the dissolution processes), overcoming the main cause of increasing δ_b. Also, the additional chemical effects (namely pH increase throughout the anodization) that limits the NTs growth and leads to a non-steady state anodization, are delayed since the anodization growth limit is postponed. We observed that the degree of ordering is highly extended by decreasing *Rq*. We developed a new method to quantify the degree on such organization including the measurement of HCPA domain areas. Large areas with an ideal structure represented by a HCPA of hexagonally arranged cells were obtained (4.32 and 6.61 μm^2 for MP and EP samples respectively), two times larger than those previously reported. Furthermore, the obtained TiO_2 NT array structures present a degree of order comparable to that of AAO templates (a porosity of 11 %).

Finally, we emphasize that by using a single anodization step with the presented optimized pre-treatments one can reach high quality TiO_2 NT arrays, with large organized domains at a reduced time and cost, making it a straightforward application on Ti foils.

Acknowledgements

A. Apolinário acknowledges the financial support under the Portuguese Foundation for Science and Technology (FCT) project PTDC/EQU-EQU/107990/2008.
L. Andrade, D.C.Leitao and C.T. Sousa are also grateful to FCT for their Post-Doc fellows (references: SFRH/BPD/74944/2010, SFRH/BPD/72359/2010 and SFRH/BPD/82010/2011, respectively). J. Ventura acknowledges financial support through FSE/POPH. The authors acknowledge funding from FCT through the PTDC/EQU-EQU/101397/2008 project and the Associated Laboratory – IN.

Notes and references

1 R. Krol, Y. Liang and J. Schoonman, *J. Mater. Chem.*, 2008, **18**, 2311; P. Song, X. Zhang, M. Sun, X. Cui and Y. Linb, *Nanoscale*, 2012, **4**, 1800.

2 X. Lu, G. Wang, T. Zhai, M. Yu, J. Gan, Y. Tong and Y. Li, *Nano Lett.*, 2012, **12**, 1690.

3 P. Xiao, B. B. Garcia, Q. Guo, D. Liu, G.Cao, *Electrochem. Commun*., 2007, **9**, 2441.

4 B.O'Regan, M. Gratzel, *Nature*, 1991, **353**, 737; M. Gratzel, *Nature*, 2001, **414**, 338.

5 P. Roy, D. Kim, K. Lee, E. Spieckerb and P. Schmuki, *Nanoscale*, 2010, **2**, 45.

6 V. Zwilling, M. Aucouturier, E. Darque-Ceretti, *Electrochimica Acta*, 1999, **45** (6), 921.

7 M. Paulose, H. E. Prakasam, O. K. Varghese, L. Peng, K. C. Popat, G. K. Mor,T. A. Desai, and C. A. Grimes, *J. Phys. Chem. C*, 2007, **111**, 14992; M. Paulose, K. Shankar, S. Yoriya, H. E. Prakasam, O. K. Varghese, G.K. Mor, T. A. Latempa, A. Fitzgerald and C. A. Grimes, *J. Phys. Chem.* B, 2006, **110,** 16179;

8 K. Shankar, G. K. Mor, H. E. Prakasam, S. Yoriya, M. Paulose, O. K. Varghese and C. A. Grimes, *Nanotechnology*, 2007, **18,** 065707.

9 V. Vega, M. A. Cerdeira, V. M. pride , D. Alberts, N. Bordel, R. Pereiro, F. F. Mera, S. Garcia, M. Hernandez-Velez, M. Vasquez, *Journal of Non-Cristaline Solids*, 2008, **354**, 5233.

10 E. Balaur, J. M. Macak, L. Taveira, P. Schmuki, *Electrochemistry Communications*, 2005, **7**, 1066.

11 H. Yin, H. Lui and W. Z. Shen, *Nanotechnology*, 2010, **21**, 035601.

12 S. Sreekantan, K. A. Saharudin, Z. Lockman, T. W. Tzu , *Nanotechnology*, 2010, **21**, 365603.

13 S. So, K. Lee, and P. Schmuki, *J. Am. Chem. Soc*., 2012, **28**, 11316; S. So, K. Lee, and P. Schmuki, *Chem. Eur. J*., 2013, **19**, 2966.

14 S. Berger, R. Hahn, P. Roy, P. Schmuki, *Phys. Status Solidi b*, 2010, **247**, 2424.

15 M. Macak, H. Tsuchiya, and P. Schmuki, *Angew. Chem. Int. Ed*., 2005, **44**, 2100.

16 L. Sun, S. Zhang , X. W. Sun and X. He, *Journal of Electroanalytical Chemistry*, **637**, 2009, 6.

17 D. Guan and Y. Wang, *Nanoscale*, 2012, **4**, 2968.
18 X. Tang, , D. Li, *J. Phys. Chem. C*, 2009, **113**, 7107.
19 S. Berger, J. Kunze, P. Schmuki, D . LeClere, A. T. Valota, P. Skeldon, G. E. Thompson, *Electrochim. Acta*, 2009, **54**, 5942.
20 Q. Y. Cai, M. Paulose, O. K. Varghese and C. A. Grimes, *J. Mater. Res.* 2005, **20**, 230.
21 V.Vega**,** Victor M. Prida**,** M. Hernández-Vélez**,** E. Manova**,** P. Aranda**,** E. Ruiz-Hitzky and Manuel Vázquez, *Nanoscale Res. Lett*., 2007, **2,** 355.
22 V.M. Prida,, V. Vega, P. Aranda,, M. Vázquez , E. Ruiz-Hitzky, J. Magn. Magn. Mater. , 2007, **316**, 110.
23 S. Kim, B. G. Lee, and J. Choi, *Bull. Korean Chem. Soc*. 2011, **32**, 3730.
24 X. Yuan, M. Zheng, L. Ma and W. Shen, *Nanotechnology*, 2010, **21**, 405302.
25 G. D. Sulka, J. Kapusta-Kołodziej, A. Brzozka, M. Jaskuła, *Electrochimica Acta* , 2010, 55, 4359.
26 K. Zhu, T. B. Vinzant, N. R. Neale, A. J. Frank, *Nano Lett.*, 2007, **7**, 3739.
27 S. P. Albu and P. Schmuki, *Phys. Stat. Sol. RRL* , 2010, **4**, 151.
28 K. Nielsch, J. Choi, K. Schwirn, R. B. Wehrspohn, and U. Gosele., *Nano Lett.*, 2002, **2**, 677.
29 J. M. Macak, S. P. Albu, and P. Schmuki, *Phys. Stat. Sol. RRL*, 2007, **1**, 181.
30 Y. Li, X. Yu and Q. Yang, *Journal of Sensors*, 2009, **2009**, 402174.
31 Y. Shin and S. Lee, *Nano Lett*., 2008, **8**, 3171.
32 D. C. Leitao, A. Apolinario, C. T. Sousa, J. Ventura, J. B. Sousa, M. Vazquez and J. P. Araujo, *J. Phys. Chem. C*, 2011, **115**, 8567.
33 B. G. Lee , S. Y. Hong, J. E. Yoo and J. Choi, *Applied Surface Science*, **257**, 2011, 7190.
34 K. Lu, Z.Tian, J. A. Geldmeier., *Electrochimica Acta*, 2011, **56,** 6014.
35 K. F. Albertin, A. Tavares, I. Pereyra, *Applied Surface Science*, 2013, **284**, 772.
36 B. Chen, K. Lu and Z. Tian, *J. Mater. Chem.*, 2011, **21**(24), 8835.
37 H. Masuda, H. Masuda, H. Asoh, M. Watanabe, K. Nishio, M. Nakao, T. Tamamura, *Adv. Mater*., 2001, **13**, 189.
38 F. Y. Li, L. Zhang, R. M. Metzger, *Chem. Mater*., 1998,**10**, 2470.
39 H. Masuda and K. Fukuda, *Science*, 1995, **268**, 1466.
40 S. Singh, W. R. T. Barden and P. Kruse, *ACS Nano*, 2008, **2**, 2453.
41 Q. Chen, D. Xu, Z. Wu and Z. Liu, *Nanotechnology*, 2008, **19**, 365708.
42 S. Bandyopadhyay, , A. E. Miller, H. C. Chang, , G. Banerjee, V. V. Yuzhakov, D. F. Yue, R. E. Ricker, S. Jones, J. A. Eastman, E. Baugher, M. Chandrasekhar, *Nanotechnology* 1996, 7, 360–371.
43 V. V. Yuzhakov, H. C. Chang, A. E. Miller, *Phys. Rev. B*, 1997, **56**, 12608.
44 V. V. Yuzhakov, P. V. Takhistov, A. E. Miller, H. C. Chang, *Chaos* 1999, **9**, 62.
45 L. B. Kong, Y. Huang, Y. Guo, H. L. Li, *Mater. Lett*. 2005, **59**, 1656.
46 D. Landolt, P. F. Chauvy, O. Zinger, *Electrochimica Acta*, 2003, **48** 3185.
47 N. Cabrera, N. F. Mott, *Rep. Prog. Phys.* 1948-1949, **12**, 163.
48 Parkhutik and Shershulsky, *J. Phys. D: Appl. Phys.*, 1992, **25**, 1258.
49 W. S. Rasband, ImageJ, US National Institutes of Health, Bethesda, Maryland, USA, http://rsb.info.nih.gov/ij/, 1997–2009.
50 A.W.Ruff, *Metallurgical and Materials transactions B*, 1974, **5**, 601.
51 K. S. Raja , M. Misra, K. Paramguru, *Electrochimica Acta*, 2005, **51**, 154.